AFAPL-TR-65-20

APPLYING THE METHOD OF CHARACTERISTICS TO ANALYZE THE FLOW FIELD OF A CHEMICALLY REACTING GAS IN A TWO-DIMENSIONAL OR AN AXISYMMETRIC NOZZLE

ROGER R. CRAIG

TECHNICAL REPORT AFAPL-TR-65-20

APRIL 1965

AIR FORCE AERO PROPULSION LABORATORY
RESEARCH AND TECHNOLOGY DIVISION
AIR FORCE SYSTEMS COMMAND
WRIGHT-PATTERSON AIR FORCE BASE, OHIO

AFAPL-TR-65-20

APPLYING THE METHOD OF CHARACTERISTICS TO ANALYZE THE FLOW FIELD OF A CHEMICALLY REACTING GAS IN A TWO-DIMENSIONAL OR AN AXISYMMETRIC NOZZLE

ROGER R. CRAIG

FOREWORD

This report was prepared by the Ramjet Component Branch, Ramjet Engine Division of the Air Force Aero Propulsion Laboratory, Research and Technology Division, Wright-Patterson Air Force Base, Ohio. The work was conducted under Task 301201, "Special Ramjets," of Project 3012, "Ramjet Technology."

The report was submitted by the author 17 February 1965.

This report has been reviewed and is approved.

RICHARD T. HEMSLEY
Colonel, USAF
Air Force Aero Propulsion Laboratory

ABSTRACT

The mathematical tools for analyzing the two-dimensional and axisymmetric flow fields of a supersonic stream in which chemical reactions are occurring have been available for several years. The numerical computations of these flow fields were not considered practical until the introduction of high-speed computers and the solution of such a problem for the one-dimensional case had been completed. Recently, a computer program was developed that applied the numerical solution of the method of characteristics with finite rate chemical reactions. This program enables one to solve two-dimensional and axisymmetric reactive flow fields. This report discusses the difficulties encountered and their solutions in the development of the computer program for the two-dimensional and axisymmetric fields. Also, the mathematics used in the program are presented.

The initial computer program was written for the simple chemical system $N_2O_4 + N_2 \rightleftharpoons 2NO_2 + N_2$. This system was chosen so that basic programming difficulties would not be concealed in a maze of chemical reactions and also because some excellent experimental data were available from the Jet Propulsion Laboratory, which could be used for comparison purposes. After completion, the program was modified to handle the combustion products of hydrogen and air and to compare the calculations with experimental data from NASA, Lewis Research Center.

Excellent agreement was obtained between the computed flow properties and the experimental data for the $N_2O_4 + N_2 \rightleftharpoons 2NO_2 + N_2$ system. Although some problems were encountered in the interpretation of the data, good agreement was obtained between the computed data and experimental data for the hydrogen-air system.

TABLE OF CONTENTS

ILLUSTRATIONS

SYMBOLS

a	speed of sound
C	characteristic direction
C_p	specific heat at constant pressure
h	specific enthalpy on common base
H_T	total enthalpy
k_b	backward reaction rate
k_f	forward reaction rate
K_c	concentration equilibr'um constant
M	Mach number
M	third body as it applies to the reactions
$\mathcal{M}$	molecular weight
n	number of species
N	number of reactions
P	pressure
R	universal gas constant
T	temperature
u	flow velocity in x direction
v	flow velocity in y direction
V	flow velocity tangent to streamline
W	species molecular weight
x	variable of rectangular coordinate system
y	variable of rectangular coordinate system
Y	mass fraction

SYMBOLS (Contd)

ϵ	constant in continuity equation (O for two-dimensional and 1 for axisymmetric flow)
η	distance normal to streamline in natural coordinate system
θ	flow direction
μ	Mach angle
ξ	distance along streamline in natural coordinate system
ν	stoichiometric coefficient
ρ	density
ϕ	fuel-to-air ratio over stoichiometric fuel-to-air ratio
Φ	initial number of moles of NO_2

SUBSCRIPTS

i, j	refers to i th and j th species
f	refers to frozen conditions
t	total conditions

SUPERSCRIPTS

r'	refers to left side of chemical reaction equation
r''	refers to right side of chemical reaction equation

SECTION I

INTRODUCTION

With the increased emphasis being placed on air-breathing propulsion, more accurate techniques must be developed for analyzing engine components. The reason for this is that, at hypersonic speeds, small changes in component performance can produce large degradations in the overall engine performance. One associated problem area is the dissociation of the combustion products and the subsequent recombination of these products in the exhaust nozzle. With an adequate analytical technique, one may be able to design the nozzle to minimize the recombination losses while still keeping the friction losses reasonable or, at the very least, be able to predict these losses.

With the introduction of high-speed computers, the calculation of recombination losses in the nozzle has received more than its share of attention. Many calculations have been done on the hydrogen-air system considering finite rate chemical reactions. The main shortcoming of these calculations was the assumption of one-dimensional flow. The limitation of the one-dimensional flow calculations is overcome, by this author, by applying the method of characteristics to a chemically reacting flow and developing an IBM-7094 computer program to handle the two-dimensional case and the axisymmetric case. Although the calculations are more time-consuming than the restrictive one-dimensional calculations, a complete picture of the entire nozzle flow field with chemical reaction is now possible.

In this report, the problems encountered in developing the computer program for the two-dimensional case and the axisymmetric case are discussed. Also, the method-of-characteristics equations are derived, and the results of the computer program are presented.

Chu (Reference 1) presented the equations for the method of characteristics for the two-dimensional and axisymmetric cases including chemical reactions. He also showed that weak disturbances in supersonic flow would propagate with the frozen speed of sound even if the flow was in chemical equilibrium.

Lick (Reference 2) presented the equations of Reference 1 in a form more useful for computational purposes but interpreted the frozen speed of sound to be that due to only the translational and rotational modes of the molecules.

Wegener and Cole (Reference 3) experimentally proved that weak disturbances in supersonic flow of a reacting gas do propagate with the frozen speed of sound. In the theoretical calculations of the frozen speed of sound, Wegener and Cole included the contribution of the vibrational degrees of freedom in the calculated frozen speed of sound. The experiments were performed very carefully, but the accuracy of the measured wave angles was not great enough to ascertain whether or not the vibration contribution to the frozen speed of sound should be included. Also, no mention was made as to why the vibrational contribution to the frozen speed of sound was included even though close agreement with the experimental results could have been obtained if it was not included.

In Reference 4, Blend examined the effect of the frequency of a sound wave on the speed with which it will propagate through a reacting mixture. At low frequencies, the sound wave

propagates at the equilibrium speed of sound and, as the frequency is increased, the sound wave travels at the frozen speed of sound, which includes the vibrational contribution to the speed of sound. As the frequency is further increased, the wave travels at a speed that does not include the vibrational contribution to the frozen speed of sound.

From these four works, it appears that there is no general agreement as to whether or not the vibrational contributions to the frozen speed of sound should be included. But, from the data of Reference 4, it appears that one must answer the question, what is the frequency of a Mach wave, before one will know what to include in the frozen speed of sound.

The present computer program for the two-dimensional and the axisymmetric cases does include the vibrational contribution to the frozen speed of sound.

SECTION II

DERIVATION OF METHOD-OF-CHARACTERISTICS EQUATIONS

For the derivation of the method of characteristics in two-dimensional or axisymmetric flow, the equations of continuity, momentum, and energy will be written in the natural coordinate system (ξ,η), see Figure 1, where ξ is the distance along a streamline and η is the distance normal to the streamline.

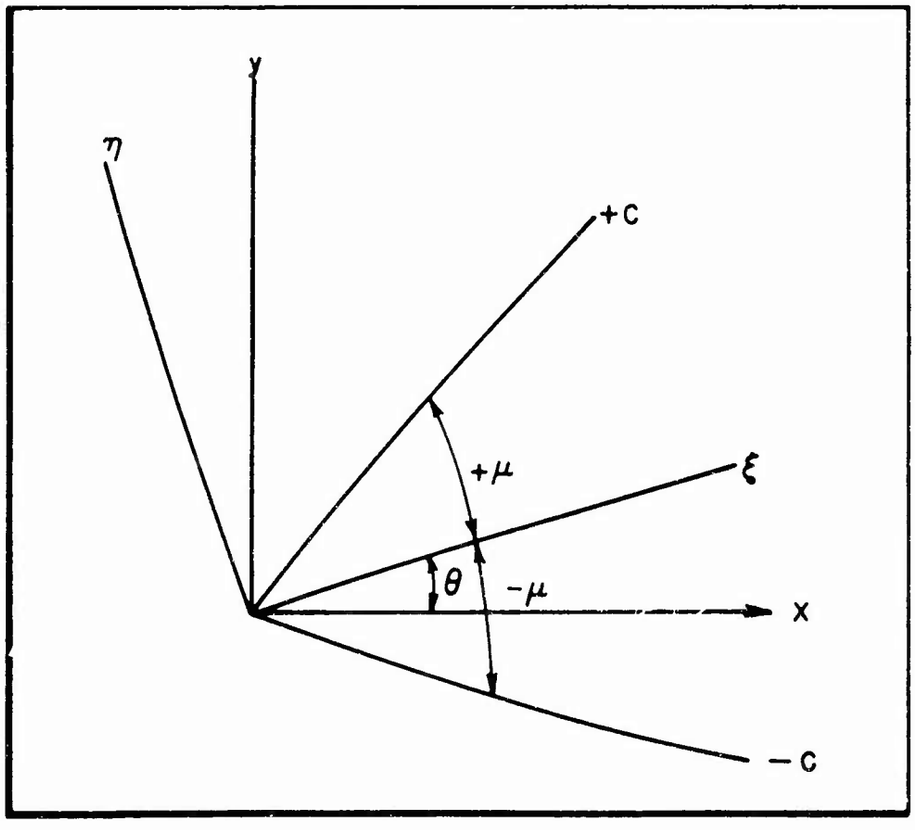

Figure 1. Coordinate System

From Reference 1 and 2, one has the following equations:

Continuity

$$\rho \frac{\partial V}{\partial \xi} + V \frac{\partial \rho}{\partial \xi} + \rho V \frac{\partial \theta}{\partial \eta} + \rho V \epsilon \frac{\sin \theta}{y} = 0 \tag{1}$$

Momentum

$$\rho V \frac{\partial V}{\partial \xi} + \frac{\partial P}{\partial \xi} = 0 \tag{2}$$

$$\rho V^2 \frac{\partial \theta}{\partial \xi} + \frac{\partial P}{\partial \eta} = 0 \tag{3}$$

Energy

$$\frac{\partial h}{\partial \xi} + V \frac{\partial V}{\partial \xi} = 0 \tag{4}$$

Rate of Species Change

$$V \frac{\partial Y_i}{\partial \xi} = \dot{Y}_i \tag{5}$$

where

$$\dot{Y}_i = \frac{W_i}{\rho} \sum_{r=1}^{N} \left(\upsilon_i^{r''} - \upsilon_i^{r'} \right) \left\{ k_f^r \prod_{j=1}^{n} \left(\frac{Y_j \rho}{W_j} \right)^{\upsilon_j^{r'}} - k_b^r \prod_{j=1}^{n} \left(\frac{Y_j \rho}{W_j} \right)^{\upsilon_j^{r''}} \right\}$$

Equation of State

$$\rho = P/RT \sum_{i=1}^{n} \frac{Y_i}{W_i} \tag{6}$$

$$\frac{\partial \rho}{\partial \xi} = \frac{\partial \rho}{\partial P} \frac{\partial P}{\partial \xi} + \frac{\partial \rho}{\partial T} \frac{\partial T}{\partial \xi} + \frac{\partial \rho}{\partial Y_i} \frac{\partial Y_i}{\partial \xi} \tag{7}$$

Substituting Equation 7 into Equation 1 gives

$$\rho \frac{\partial V}{\partial \xi} + \frac{\rho V}{P} \frac{\partial P}{\partial \xi} - \frac{\rho V}{T} \frac{\partial T}{\partial \xi} - \frac{\rho V}{\sum_{i=1}^{n} Y_i / W_i} \sum_{i=1}^{n} \frac{1}{W_i} \frac{\partial Y_i}{\partial \xi} \tag{8}$$

$$+ \rho V \frac{\partial \theta}{\partial \eta} + \rho V \epsilon \frac{\sin \theta}{y} = 0$$

$$h = \sum_{i=1}^{n} h_i Y_i \tag{9a}$$

$$\frac{\partial h}{\partial \xi} = \sum_{i=1}^{n} h_i \frac{\partial Y_i}{\partial \xi} + \sum_{i=1}^{n} Y_i \frac{\partial h_i}{\partial \xi} \tag{9b}$$

where

$$\frac{\partial h_i}{\partial \xi} = \frac{\partial h_i}{\partial T} \frac{\partial T}{\partial \xi} = c_{p_i} \frac{\partial T}{\partial \xi}$$

Combining Equations 9a, 9b, and 4 gives

$$\frac{\partial T}{\partial \xi} = - \sum_{i=1}^{n} \frac{n_i}{c_p} \frac{\partial Y_i}{\partial \xi} - \frac{V}{c_p} \frac{\partial V}{\partial \xi} \tag{10}$$

Substituting Equation 10 into Equation 8 gives

$$\rho \frac{\partial V}{\partial \xi} + \frac{\rho V}{P} \frac{\partial P}{\partial \xi} + \frac{\rho V}{T} \sum_{i=1}^{n} \frac{h_i}{c_p} \frac{\partial Y_i}{\partial \xi} + \frac{\rho V^2}{c_p T} \frac{\partial V}{\partial \xi} \tag{11}$$

$$- \frac{\rho V}{\sum_{i=1}^{n} Y_i / W_i} \sum_{i=1}^{n} \frac{1}{W_i} \frac{\partial Y_i}{\partial \xi} + \rho V \frac{\partial \theta}{\partial \eta} + \rho V \epsilon \frac{\sin \theta}{y} = 0$$

Eliminating $\frac{\partial V}{\partial \xi}$ in Equation 11 by use of Equation 2, one obtains

$$- \frac{1}{V} \frac{\partial P}{\partial \xi} + \frac{\rho V}{P} \frac{\partial P}{\partial \xi} + \frac{\rho V}{T} \sum_{i=1}^{n} \frac{h_i}{c_p} \frac{\partial Y_i}{\partial \xi} - \frac{V}{c_p T} \frac{\partial P}{\partial \xi}$$

$$- \frac{\rho V}{\sum_{i=1}^{n} Y_i / W_i} \sum_{i=1}^{n} \frac{1}{W_i} \frac{\partial Y_i}{\partial \xi} + \rho V \frac{\partial \theta}{\partial \eta} + \rho V \epsilon \frac{\sin \theta}{y} = 0$$

Replacing $\frac{\partial Y_i}{\partial \xi}$ by Equation 5 gives

$$-\frac{1}{V}\frac{\partial P}{\partial \xi} + \frac{\rho V}{P}\frac{\partial P}{\partial \xi} + \rho V \sum_{i=1}^{n} \frac{h_i}{C_p T V}\dot{Y}_i - \frac{V}{C_p T}\frac{\partial P}{\partial \xi} \tag{12}$$

$$-\rho V \sum_{i=1}^{n} \frac{m}{W_i V}\dot{Y}_i + \rho V \frac{\partial \theta}{\partial \eta} + \rho V \epsilon \frac{\sin\theta}{y} = 0$$

One must also utilize the following relations:

$$dP = \frac{\partial P}{\partial \xi} d\xi + \frac{\partial P}{\partial \eta} d\eta \tag{13}$$

$$d\theta = \frac{\partial \theta}{\partial \xi} d\xi + \frac{\partial \theta}{\partial \eta} d\eta \tag{14}$$

Equations 3, 12, 13, and 14 are a system of equations for the unknowns $\partial P/\partial \xi$, $\partial P/\partial \eta, \partial \theta/\partial \xi, \partial \theta/\partial \eta$ and have a unique solution unless, when the system is solved for one of the unknowns, the value of determinant of the coefficients for the solution is zero.

To reduce the problem to the solution of ordinary differential equations, we require that the equations be linearly dependent along some characteristic curve. If this is true, then at least one of the variables is arbitrary and hence may be discontinuous along the characteristic curve. For one variable to be discontinuous, we solve for its value and set the determinant of the coefficient of the numerator equal to zero since we have assumed the equations to be linearly dependent and the determinant of the denominator is necessarily zero.

Letting $A = \rho V/P - 1/V - V/C_p T$ and setting up the determinant of the coefficients of the variable, one obtains

$$\begin{array}{cccc} \frac{\partial P}{\partial \xi} & \frac{\partial P}{\partial \eta} & \frac{\partial \theta}{\partial \xi} & \frac{\partial \theta}{\partial \eta} \\ \left| \begin{array}{cccc} A & 0 & 0 & \rho V \\ 0 & 1 & \rho V^2 & 0 \\ d\xi & d\eta & 0 & 0 \\ 0 & 0 & d\xi & d\eta \end{array} \right| \end{array} = 0 = A\rho V^2 d\eta^2 + \rho V d\xi^2$$

$$\frac{d\eta}{d\xi} = \pm \frac{1}{\sqrt{AV}} = \pm \frac{1}{\sqrt{(\rho V/P - 1/V - V/C_p T)V}}$$

$$\frac{d\eta}{d\xi} = \pm \frac{1}{\sqrt{\frac{\gamma V^2}{RT}\frac{V^2}{C_p T} - 1}} = \pm \frac{1}{\sqrt{\frac{\gamma C_p - R}{C_p R T} V^2 - 1}}$$

Since

$$a_f^2 = C_p R T / \left[\gamma C_p - R\right]$$

then

$$\frac{d\eta}{d\xi} = \pm 1/\sqrt{V^2/a_f^2 - 1} = \pm 1/\sqrt{M_f^2 - 1}$$

The rate of change of η with respect to ξ along the characteristic curve is defined as the tangent of the Mach angle and is the slope of the characteristic curve or

$$\frac{d\eta}{d\xi} = \pm \text{Tan } \mu_f \tag{15}$$

Now setting up the numerator determinant and putting its value equal to zero, we can determine our other equation. It does not matter which variable one solves for, since the same answer will be obtained for any variable. Choosing the determinant for $\partial P/\partial \eta$ and letting

$$B = \rho V \sum_{i=1}^{n} \frac{\gamma}{W_i} \dot{Y}_i - \rho V \sum_{i=1}^{n} \frac{h_i}{C_p T V} \dot{Y}_i - \rho V \epsilon \frac{\sin \theta}{y}$$

gives

$$\begin{vmatrix} A & B & 0 & \rho V \\ 0 & 0 & \rho V^2 & 0 \\ d\xi & dP & 0 & 0 \\ 0 & d\theta & d\xi & d\eta \end{vmatrix} = 0$$

Expanding the determinant, one has

$$- A\,d\eta\,dP\rho V^2 + d\xi \left[B\rho V^2\, d\eta - d\theta\, \rho^2 V^3 \right] = 0$$

and dividing by $\rho^2 V^3\, d\eta$ and changing signs gives

$$\frac{AV}{\rho V^2}\, dP + d\theta \frac{d\xi}{d\eta} = \frac{B}{\rho V}\, d\xi$$

Since

$$\left(\frac{d\eta}{d\xi}\right)^2 = \frac{1}{AV} = \tan^2 \mu_f$$

then

$$\frac{dP}{\tan^2 \mu_f\, \rho V^2} \pm \frac{d\theta}{\tan \mu_f} = B \frac{d\xi}{\rho V}$$

$$\frac{dP}{\tan \mu_f\, \rho V^2} \pm d\theta = \frac{\tan \mu_f\, d\xi}{\rho V} B$$

If dc is the distance along the characteristic curve, one has

$$d\xi = dc \cos \mu_f$$

$$\frac{dP}{\rho V^2 \tan \mu_f} \pm d\theta = \sin \mu_f\, dc\, B$$

but

$$\pm \tan \mu_f = 1/\sqrt{M_f^2 - 1}$$

therefore

$$\sin \mu_f = \frac{1}{M_f} = a_f/V$$

$$\frac{dP}{\rho V^2 \tan \mu_f} \pm d\theta = \frac{a_f}{V} dc \left[- \frac{\epsilon \sin \theta}{y} - \sum_{i=1}^{n} \frac{h_i}{C_p T V} \dot{Y}_i + \sum_{i=1}^{n} \frac{m}{W_i V} \dot{Y}_i \right] \quad (16)$$

To change from ξ, η coordinate system, reference is made to a diagram of the flow field, see Figure 1. Since $d\eta/d\xi$ along the characteristic curve dc is $\pm \tan \mu_f$, dy/dx along the characteristic curve must be $\tan(\theta \pm \mu_f)$. The system of differential equations is now:

Along Characteristics

$$\frac{d_y}{d_x} = \tan (\theta \pm \mu_f) \quad (17)$$

$$\frac{dP}{\rho V^2 \tan \mu_f} \pm d\theta = \frac{a_f}{V} dc \left[- \frac{\epsilon \sin \theta}{y} - \sum_{i=1}^{n} \frac{h_i}{C_p T V} \dot{Y}_i + \sum_{i=1}^{n} \frac{m}{W_i V} \dot{Y}_i \right] \quad (18)$$

Along Streamlines

$$VdV + dP/\rho = 0 \quad (19)$$

$$udy - vdx = 0 \quad (20)$$

$$VdY_i = \dot{Y}_i \, d\xi \quad (21)$$

The total enthalpy is assumed to be the same everywhere in the flow field

$$H_t = h + V^2/2$$

To solve the equations, we must set the equations up in a finite difference form and start with an initial line of data that is not along a characteristic line. In finite difference forms, the equations are along the characteristic

$$\frac{\Delta y}{\Delta x} = \tan \left[\bar{\theta} \pm \bar{\mu}_f \right]$$

where the bars over the symbols denote average values between two points (see Figure 2):

$$\frac{\Delta P}{\bar{\rho} \bar{V}^2 \tan \bar{\mu}_f} \pm \Delta\theta = \frac{\bar{a}_f}{\bar{V}} \Delta c \left[- \frac{\epsilon \sin \bar{\theta}}{\bar{y}} - \sum_{i=1}^{n} \overline{\frac{h_i}{C_p T V}} \dot{Y}_i + \sum_{i=1}^{n} \overline{\frac{m}{W_i V}} \dot{Y}_i \right]$$

Along the streamlines, we have

$$\bar{V} \Delta V + \frac{\Delta P}{\bar{\rho}} = 0$$

$$\frac{\Delta y}{\Delta x} = \frac{\bar{v}}{\bar{u}}$$

where

$$V = \sqrt{u^2 + v^2}$$

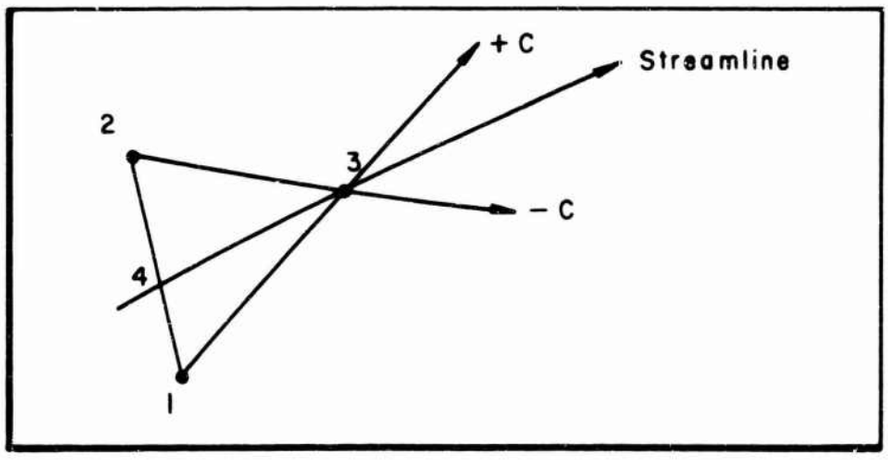

Figure 2. Flow Field

To find the location of the next point on our characteristic from two initial points, the difference equations are set up and solved simultaneously as follows:

$$\frac{y_3 - y_1}{x_3 - x_1} = \tan \overline{(\theta + \mu_f)}_{3-1}$$

$$\frac{y_3 - y_2}{x_3 \quad x_2} = \tan \overline{(\theta - \mu_f)}_{3-2}$$

where the subscripts 3-1 and 3-2 indicate between which two points the average value is to be taken. Thus

$$x_3 = \frac{y_2 - y_1 - x_2 \tan \overline{(\theta - \mu_f)}_{3-2} + x_1 \tan \overline{(\theta + \mu_f)}_{3-1}}{\tan \overline{(\theta + \mu_f)}_{3-1} - \tan \overline{(\theta - \mu_f)}_{3-2}}$$

$$y_3 = y_1 + (x_3 - x_1) \tan \overline{(\theta + \mu_f)}_{3-1}$$

Now letting

$$A_1 = \overline{(\rho V^2 \tan \mu_f)}_{3-1}$$

$$A_2 = \overline{(\rho V^2 \tan \mu_f)}_{3-2}$$

$$B_1 = \sin \bar{\mu}_{f_{3-1}} \; \Delta C_{3-1} \left[-\left(\frac{\overline{\epsilon \sin \theta}}{y} \right)_{3-1} - \left(\sum_{i=1}^{n} \frac{h_i}{C_p T V} \dot{Y}_i \right)_{3-1} + \left(\sum_{i=1}^{n} \frac{m}{W_i V} \dot{Y}_i \right)_{3-1} \right]$$

$$\Delta C_{3-1} = \sqrt{(x_3 - x_1)^2 + (y_3 - y_1)^2}$$

$$B_2 = \sin \bar{\mu}_{f_{3-2}} \; \Delta C_{3-2} \left[- \left(\frac{\overline{\epsilon \sin \theta}}{y} \right)_{3-2} - \left(\sum_{i=1}^{n} \frac{h_i}{C_p T V} \dot{Y}_i \right)_{3-2} + \left(\sum_{i=1}^{n} \frac{m}{W_i V} \dot{Y}_i \right)_{3-2} \right]$$

$$\Delta C_{3-2} = \sqrt{(x_3 - x_2)^2 + (y_3 - y_2)^2}$$

finally one has

$$\frac{P_3 - P_1}{A_1} + \theta_3 - \theta_1 = B_1$$

$$\frac{P_3 - P_2}{A_2} - \theta_3 + \theta_2 = B_2$$

$$P_3 = \frac{B_1 + B_2 + \theta_1 - \theta_2 + P_1/A_1 + P_2/A_2}{1/A_1 + 1/A_2}$$

$$\theta_3 + B_1 + \theta_1 - \left(\frac{P_3 - P_1}{A_1} \right)$$

One also knows that the streamline passing through Point 3 starts from some point between 1 and 2. This point can be found using the following relations along a streamline

$$\frac{\Delta y}{\Delta x} = \frac{\bar{v}}{\bar{u}}$$

$$\bar{V} \Delta V + \Delta P / \bar{\rho} = 0$$

Assuming a location for the streamline origin, one linearly interpolates between the conditions at 1 and 2 to find the conditions at the origin of the streamline. Then

$$V_3 = \frac{V_4 - \dfrac{P_3 - P_4}{\bar{\rho}_{3-4}}}{\bar{V}_{3-4}}$$

where 3-4 indicates that the average value is taken between Points 3 and 4 of Figure 2. Since we know θ_3, we can find u_3 and v_3 and check to see if

$$\frac{y_3 - y_4}{x_3 - x_4} = \frac{\bar{v}_{3-4}}{\bar{u}_{3-4}}$$

This is continued until the preceding relation is satisfied. Then from

$$\frac{\Delta Y_i}{\Delta \xi} = \frac{\dot{Y}_i}{\bar{V}_{3-4}} \quad \text{and} \quad \Delta \xi = \sqrt{(x_3 - x_4)^2 + \left[y_3 - y_4\right]^2}$$

one can determine the mass fractions at 3. All conditions at 3 are now known. The process is then continued for the entire flow field.

SECTION III

INITIAL COMPUTER PROGRAM FOR THE $N_2O_4 + N_2 \rightleftharpoons 2NO_2 + N_2$ SYSTEM

PROBLEMS ENCOUNTERED

The initial computer program was written for the system $N_2O_4 + N_2 \rightleftharpoons 2NO_2 + N_2$ so that errors in the characteristic equations would not be concealed in a maze of chemical equations. The initial computations were for the two-dimensional case. The nozzle described in Reference 5 was used in the calculations.

To start the method-of-characteristics calculations, one must know the conditions at various points on an initial data line that is not a characteristic line. For the two-dimensional nozzle considered, we used one-dimensional calculations with finite reactions rates to obtain this data. For a point close to the throat, the conditions on the initial data line were assumed to be the same as the one-dimensional case. Because of the low divergence angle of the nozzle in Reference 5, this is a good approximation.

Also, since finite difference techniques are used, average values of the variables must be used in the equations and one must assume initially that the flow properties at the point being solved for are the same as at the initial point. One can then solve for P, θ and all other variables at the new point and use their new values to find the average values for the next calculation. This procedure was then repeated until consecutively calculated pressures agreed within 0.1 percent. The only problem encountered in these calculations was that the rates of change of the species mass fractions were so rapid that finite differences could not be used to obtain the mass fractions at the new point.

Since one has already calculated, at least to a first approximation, the values of x, y, P, θ, and V at the new point in the flow field, this problem can be circumvented. If one connects the two initial points by a straight line, the point on this line, from which the streamline passing through the new point originates, can be found. The mass fractions can then be found by numerical integration of Equation 21. To perform this numerical integration, one must know the temperature, density, and velocity along this approximate streamline. These can be found by first assuming that the specific heat and molecular weight at the new point are the same as at the original point, or

$$(C_p)_3 = (C_p)_1$$

$$m_3 = m_1$$

Then

$$T_3 = T_1 + \frac{V_1^2 - V_3^2}{2\,C_p}$$

$$\rho_3 = \rho_1 \frac{P_1}{T_1} \frac{T_3}{P_3}$$

Next one assumes that T, ρ, and V vary linearly along this streamline and one can then numerically integrate the equation for the change in mass fractions. This must be done for every iteration during the search for P_3 and is the most time consuming part of the program.

COMPARISON OF EXPERIMENTAL DATA WITH CALCULATED RESULTS

Since the nozzle of Reference 5 had a very small expansion angle (~1.15 degrees), one would expect the flow to be nearly one-dimensional so that the method-of-characteristics calculations should be very close to the one-dimensional calculations. As can be seen in Figures 3 through 6, this is the case.

Figure 3 compares the experimental pressure distribution for the two-dimensional flow with that calculated one-dimensionally and by the method of characteristics. The agreement is quite good.

Figure 4 shows the theoretical temperature distribution through the nozzle, although no experimental temperature measurements were made. One can see that even though the pressure distribution indicated that the flow is in equilibrium, the temperature distribution indicates a slight departure from equilibrium.

Figure 5 is a comparison of the experimental and theoretical concentration ratio of NO_2. The experimental accuracy of these measurements is not as great as for the pressure measurements but the agreement is still satisfactory.

Figure 6 shows the theoretical distribution of the mass fractions of NO_2.

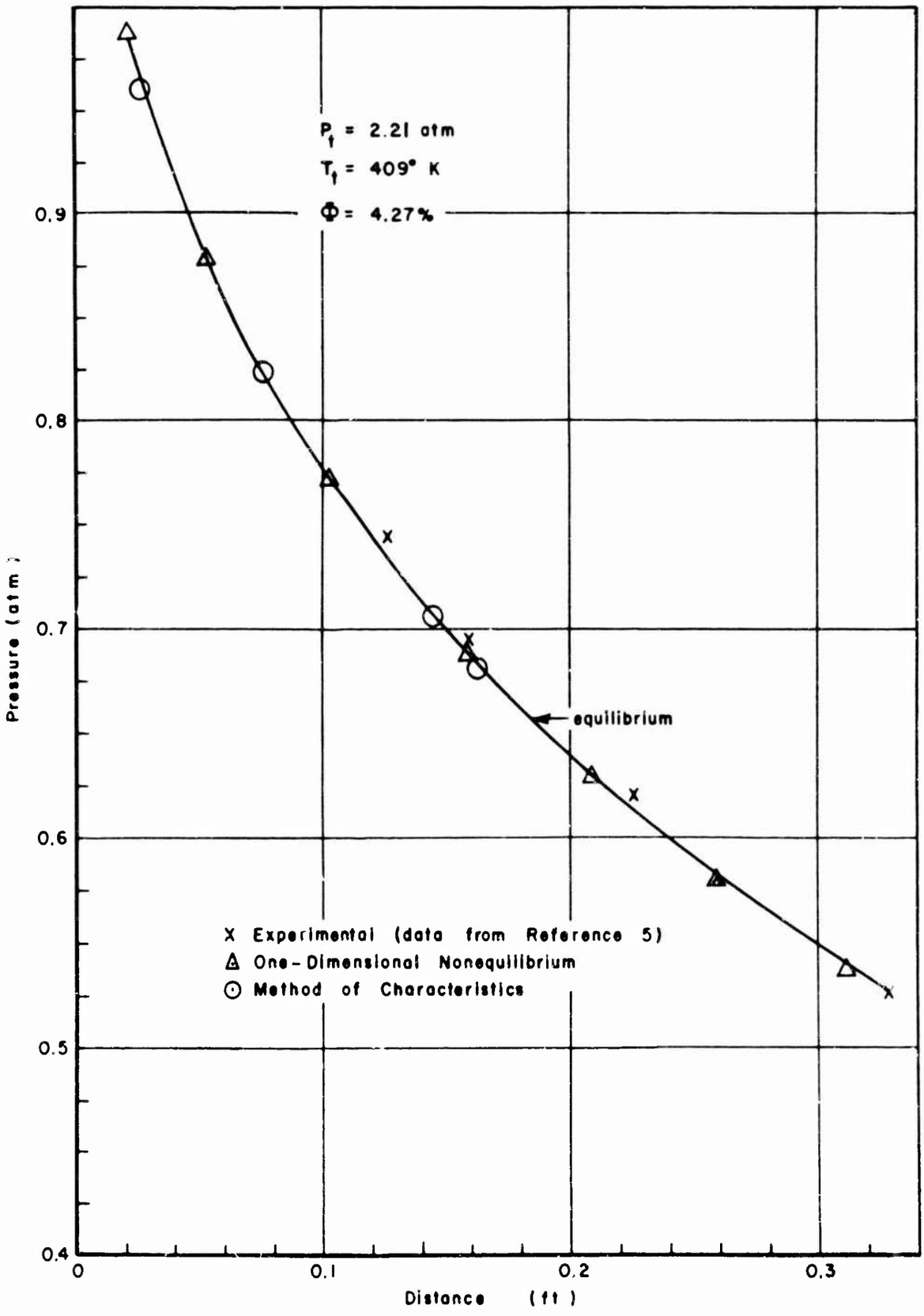

Figure 3. Nozzle Wall Pressure versus Distance Using Two-Dimensional Nozzle Geometry from Reference 5

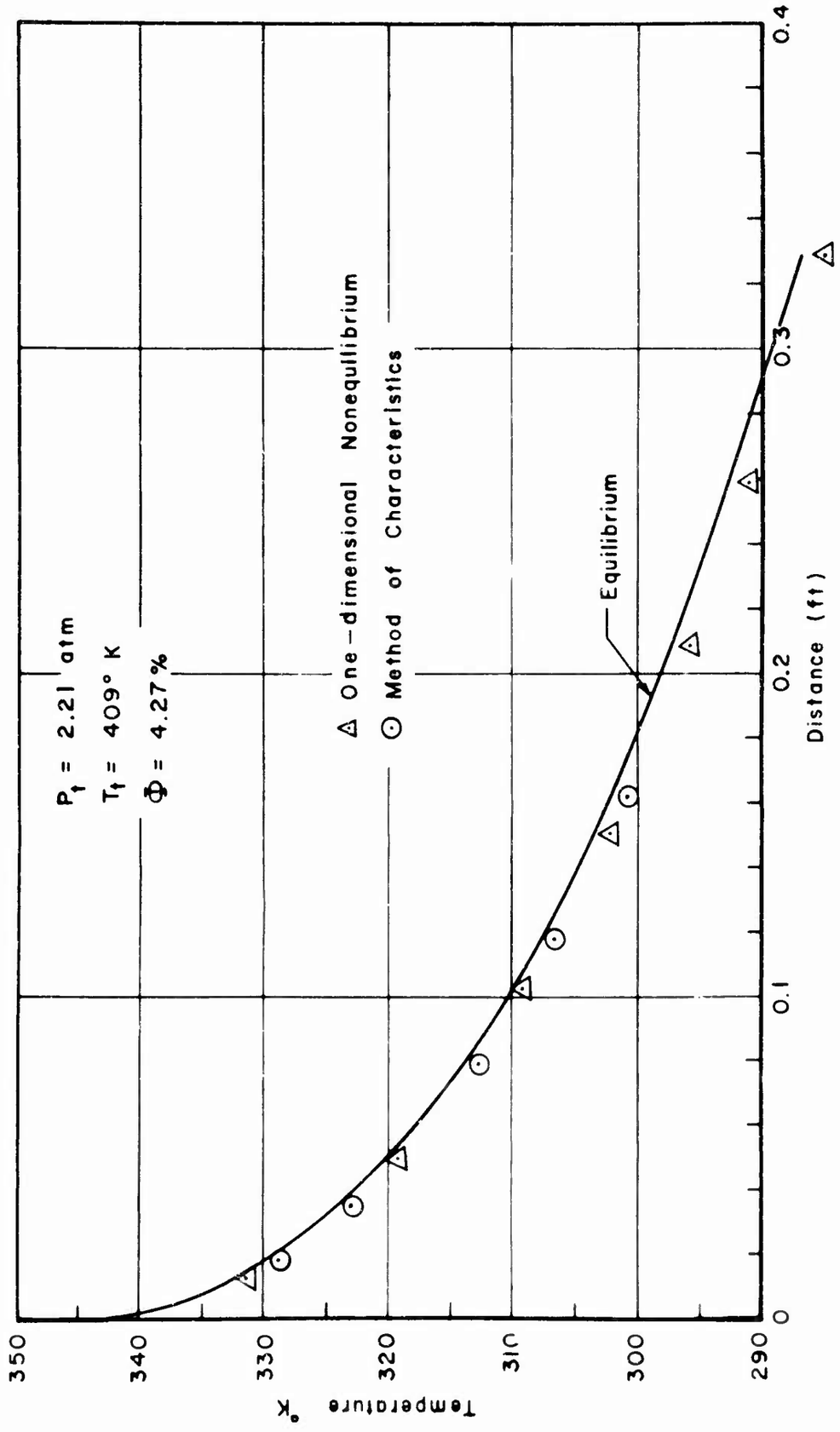

Figure 4. Temperature at Nozzle Wall versus Distance Using Two-Dimensional Nozzle Geometry from Reference 5

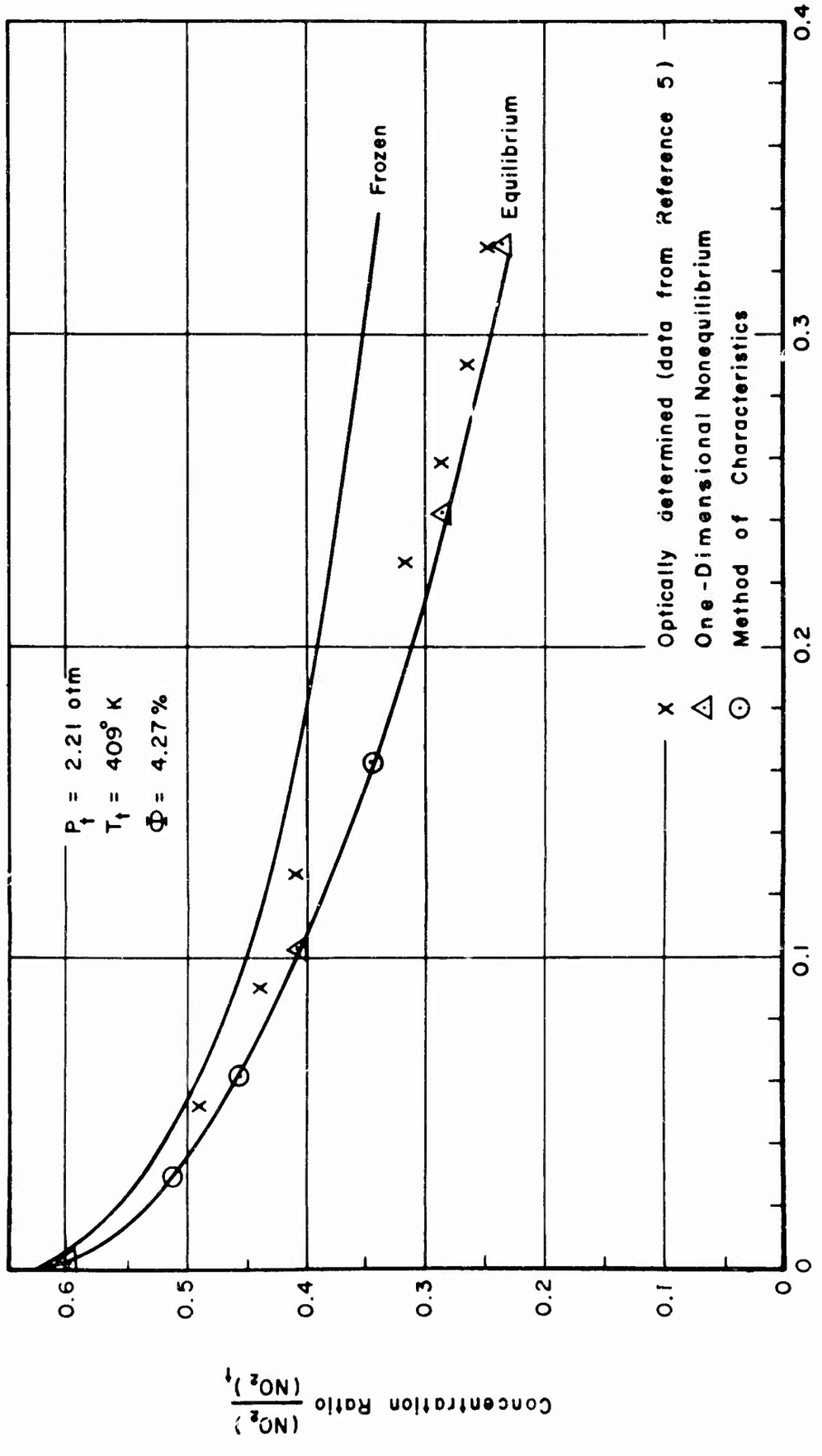

Figure 5. Concentration Ratio $\frac{(NO_2)}{(NO_2)_t}$ versus Distance Using Two-Dimensional Nozzle Geometry from Reference 5

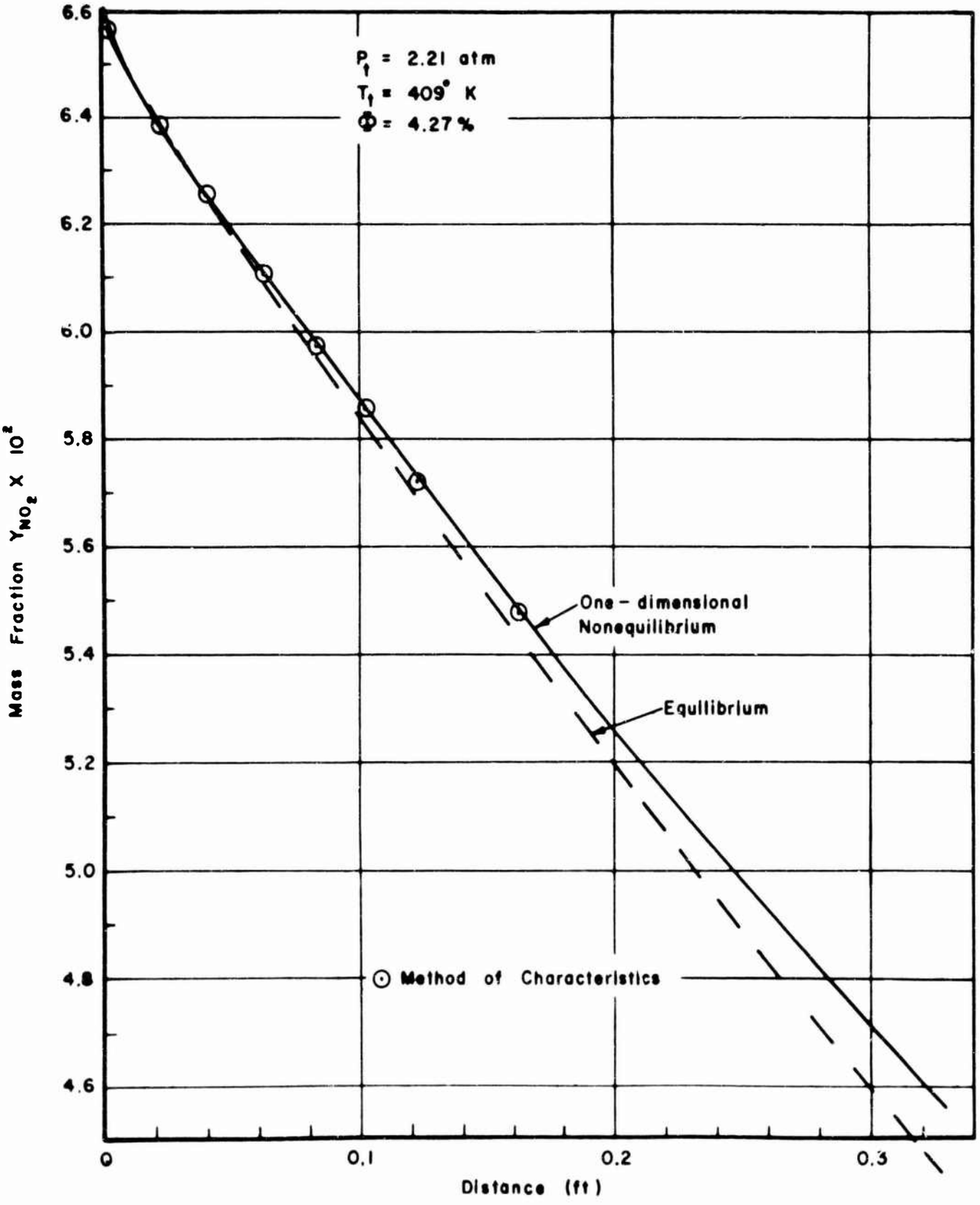

Figure 6. Mass Fraction $Y_{NO_2} \times 10^2$ versus Distance Using Two-Dimensional Nozzle Geometry from Reference 5

SECTION IV

MODIFICATION OF COMPUTER PROGRAM FOR THE HYDROGEN-AIR SYSTEM

REACTIONS CONSIDERED AND THEIR RATES

For the hydrogen-air system, 14 reactions were assumed to be occurring among the 9 species considered. The 14 reactions were assumed to be simultaneously occurring in the flow stream. These reactions and their rates are:

Reaction No.	Chemical Reaction
1	$H_2 + O_2 \rightleftharpoons OH + OH$
2	$H + O_2 \rightleftharpoons OH + O$
3	$O + H_2 \rightleftharpoons OH + H$
4	$OH + H_2 \rightleftharpoons H_2O + H$
5	$OH + OH \rightleftharpoons H_2O + O$
6	$H + H + M \rightleftharpoons H_2 + M$
7	$H + OH + M \rightleftharpoons H_2O + M$
8	$H + O + M \rightleftharpoons OH + M$
9	$O + O + M \rightleftharpoons O_2 + M$
10	$N + N + M \rightleftharpoons N_2 + M$
11	$N + O + M \rightleftharpoons NO + M$
12	$N + O_2 \rightleftharpoons NO + O$
13	$N_2 + O \rightleftharpoons NO + N$
14	$N_2 + O_2 \rightleftharpoons 2NO$

The M refers to some third body.

The reaction rates for reactions 1 through 8 were taken from Reference 6 and the rates for reactions 9 through 14 were obtained from Reference 7. These rates are:

Rate	Unit
$k_{f1} = 1 \times 10^{14} \exp(-35229/T^\circ K)$	$\frac{cm^3}{mole\text{-}sec.}$
$k_{f2} = 3 \times 10^{14} \exp(-8810/T^\circ K)$	"
$k_{f3} = 3 \times 10^{14} \exp(-4030/T^\circ K)$	"
$k_{f4} = 3 \times 10^{14} \exp(-3020/T^\circ K)$	"
$k_{f5} = 3 \times 10^{14} \exp(-3020/T^\circ K)$	"
$k_{f6} = 5 \times 10^{15}$	$\frac{cm^6}{mole^2\text{-}sec.}$
$k_{f7} = 1 \times 10^{17}$	"
$k_{f8} = 1 \times 10^{16}$	"
$k_{f9} = 3 \times 10^{14}$	"
$k_{f10} = 3 \times 10^{14}$	"
$k_{f11} = 6 \times 10^{14}$	"
$k_{f12} = 3.2 \times 10^{12}\left(\frac{T^\circ K}{1000}\right)^{1/2} \exp(-3120/T^\circ K)$	$\frac{cm^3}{mole\text{-}sec.}$
$k_{f13} = 5 \times 10^{13} \exp(-37790/T^\circ K)$	"
$k_{f14} = 2.7 \times 10^{13} \exp(-53842/T^\circ K)$	"

and

$$k_{bi} = k_{fi}/K_c$$

where i refers to the reaction number.

In the extension of the program to the hydrogen-air system, the calculations were for the axisymmetric case. Since the consideration of this number of species increased the numerical integration time by a large amount over that required for the N_2O_4 system, a major effort was made to reduce this time to a minimum.

Because numerical integration requires the calculation of the reaction rates at a large number or subintervals in any given interval and, comparatively speaking, exponential functions require a long computation time, an examination was made to see which reaction rates could be written in terms of other reaction rates. By minor changes in the exponential

factors in the rates k_{f1}, k_{f13}, and k_{f14}, one can write these reaction rates in terms of k_{f2} and k_{f3}. One now has

$$k_{f1} \doteqdot 1 \times 10^{14} \exp(-35240 / T°K) = 1 \times 10^{14} \left[\frac{k_{f2}}{3 \times 10^{14}}\right]^4$$

$$k_{f13} \doteqdot 5 \times 10^{13} \exp(-37770 / T°K) = 5 \times 10^{13} \left[\frac{k_{f2}}{3 \times 10^{14}}\right]^2 \left[\frac{k_{f3}}{3 \times 10^{14}}\right]^5$$

$$k_{f14} \doteqdot 2.7 \times 10^{13} \exp(-53890 / T°K) = 2.7 \times 10^{13} \left[\frac{k_{f2}}{3 \times 10^{14}}\right]^2 \left[\frac{k_{f3}}{3 \times 10^{14}}\right]^9$$

One other means of reducing the integration time is to combine as many terms as possible in the equations for the rates of change of each species. For the 9 species and 14 reactions considered, there are 88 terms in the equations for the rates of change of all the species, each term contains approximately 3 multiplications. Of these 88 terms, only 40 are independent of the other terms so that by combining the terms one can save 192 multiplications in each integration subinterval.

The next problem was to find the proper combination of specified accuracy on the pressure and mass fractions that would produce accurate answers and the shortest running times. It was found that when specifying 5 places accuracy on the pressure and mass fractions, the program required 15 to 20 iterations to converge on the pressure. When the accuracy on the pressure was decreased to 3 significant figures, only 2 to 3 iterations were required and the answers were essentially the same for both cases. Also, suprisingly enough, decreasing the accuracy on the mass fractions increased the number of iterations required to converge on the pressure. Thus 5 places accuracy was retained on the mass fractions.

PROBLEMS ENCOUNTERED IN STARTING THE SOLUTION

The next step was to compare the calculations with the experimental data of Reference 8. The first attempt at obtaining the conditions on the initial data line was to follow the same procedure as for the N_2O_4 system. Upon proceeding in this manner, disturbances were noticed in the solution after only a few points downstream of the initial data line. These disturbances were carried through the flow field grid until they produced a discontinuity in the center line pressure at a distance of 0.1 foot downstream of the throat. This prompted a closer look into the flow in the throat region. It was found that Reference 9 provided a very convenient analytic solution for the flow in this region. To gain confidence in the accuracy of the equations developed in Reference 9, we computed the location and shape of the sonic line for the cold flow calibration tests of Reference 8. The surface area of revolution of the sonic line was found to be 0.0548 square foot whereas the geometric throat area was 0.0517 square foot. Using the sonic line surface area and the measured total temperature and pressure of 543°R and 6892 pounds per square foot, respectively, we computed the theoretical mass flow to be 8.664 pounds per second whereas the measured mass flow was 8.637 pounds per second, a difference on only 0.13 percent.

The transonic equations were used to compute the coordinates for the Mach number of 1.2 line and to start the solution along this line. Because of the parabolic shape of this line,

there was a sudden change in grid size at the center line downstream of the starting point. This sudden change in grid size produced erroneous results at the station at which this occurred.

The next step was to assume a straight initial data line and then to compute the Mach number on this line at 11 equally spaced points. The initial data at each of these points was taken to be the same as that obtained from the one-dimensional analysis at the same Mach number as that at the point of the data line. This eliminated the problem of the sudden grid size change and produced smooth curves.

COMPARISON OF EXPERIMENTAL DATA WITH CALCULATED RESULTS

The comparison of the theoretical and experimental results for the hydrogen-air system are presented in Figures 7 through 15. The computed results are compared with the experimental results obtained from the nozzle of Reference 8. The physical measurements of the nozzle are shown in Figure 7. The locations of the static pressure taps are shown in the throat region along with the optical port locations at which static temperature measurements were made.

Figure 8 shows the nozzle contour in the throat region and gives the equation used to describe this contour.

Figure 9 shows a portion of the characteristic net generated by the program.

Figure 10 shows a comparison of the pressure distribution obtained by the method of characteristics with the experimental data and with a one-dimensional analysis. One of the main difficulties in performing this comparison was in obtaining the location of the static taps as is indicated by the bar lines. The "kink" in the wall pressure distribution obtained by the method of characteristics is due to the discontinuity in the second derivative of the equations used to describe the wall shape; it will occur in any similar case even though the slope of the wall is continuous. This discontinuity will produce a shock wave downstream of this position in the theoretical analysis, but in the physical situation this discontinuity appears to be smoothed over by the boundary layer (Reference 10).

Figure 11 shows the computed temperature distribution along with the experimental points and the one-dimensional temperature distribution. Since the experimental temperatures were determined by the sodium-D line reversal method, one does not obtain a temperature at the wall or centerline, but an average temperature of the stream. Therefore, the only conclusion one can reach for an axisymmetric nozzle is that the measured temperature should be somewhere between the calculated stream temperature at the wall and at the centerline.

Figures 12 through 15 show comparisons of the mass fractions of H, OH, H_2, and H_2O obtained by the method of characteristics with those calculated one-dimensionally.

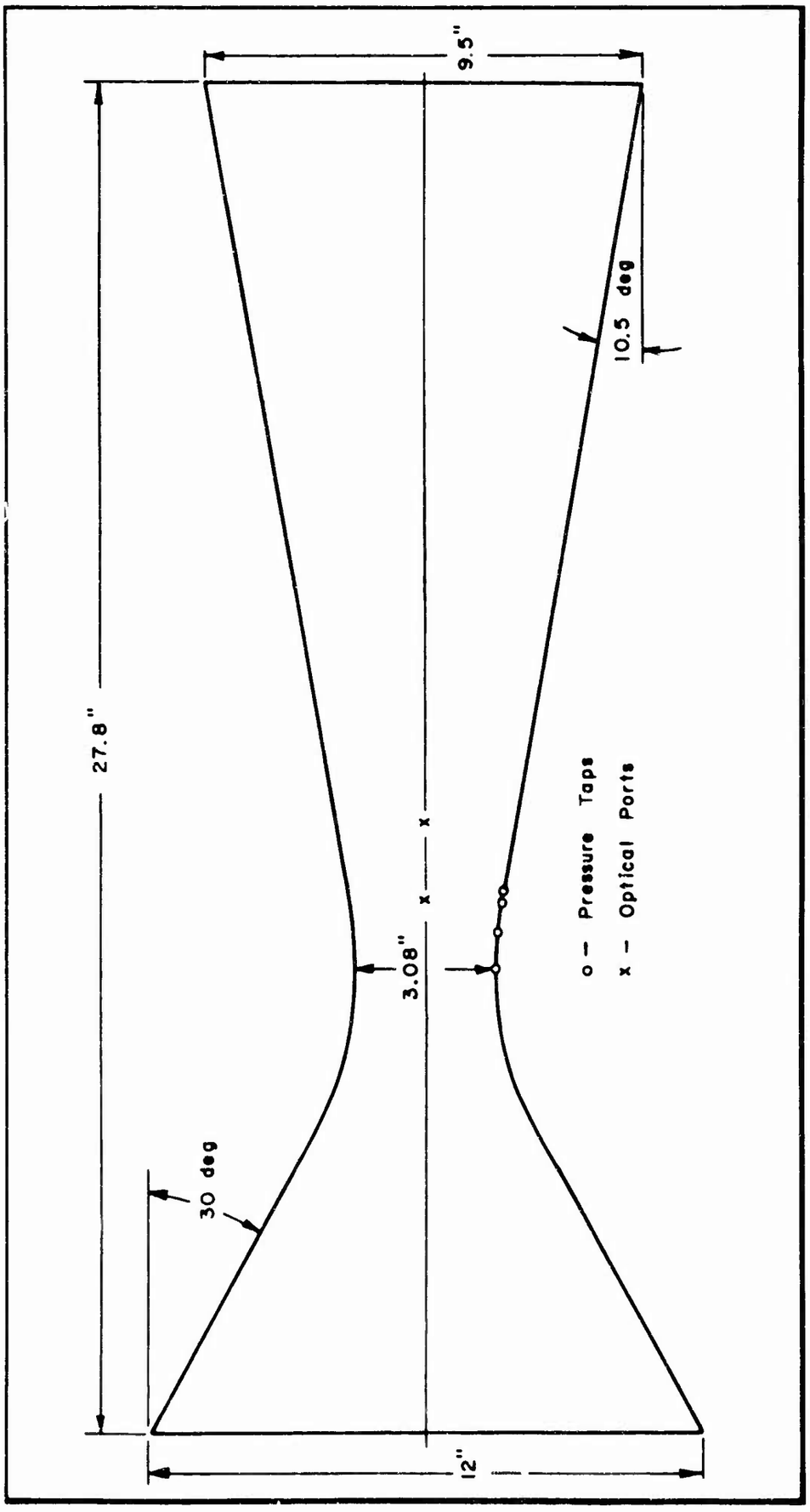

Figure 7. Dimensions of Nozzle Used for Axisymmetric Flow Field Calculations

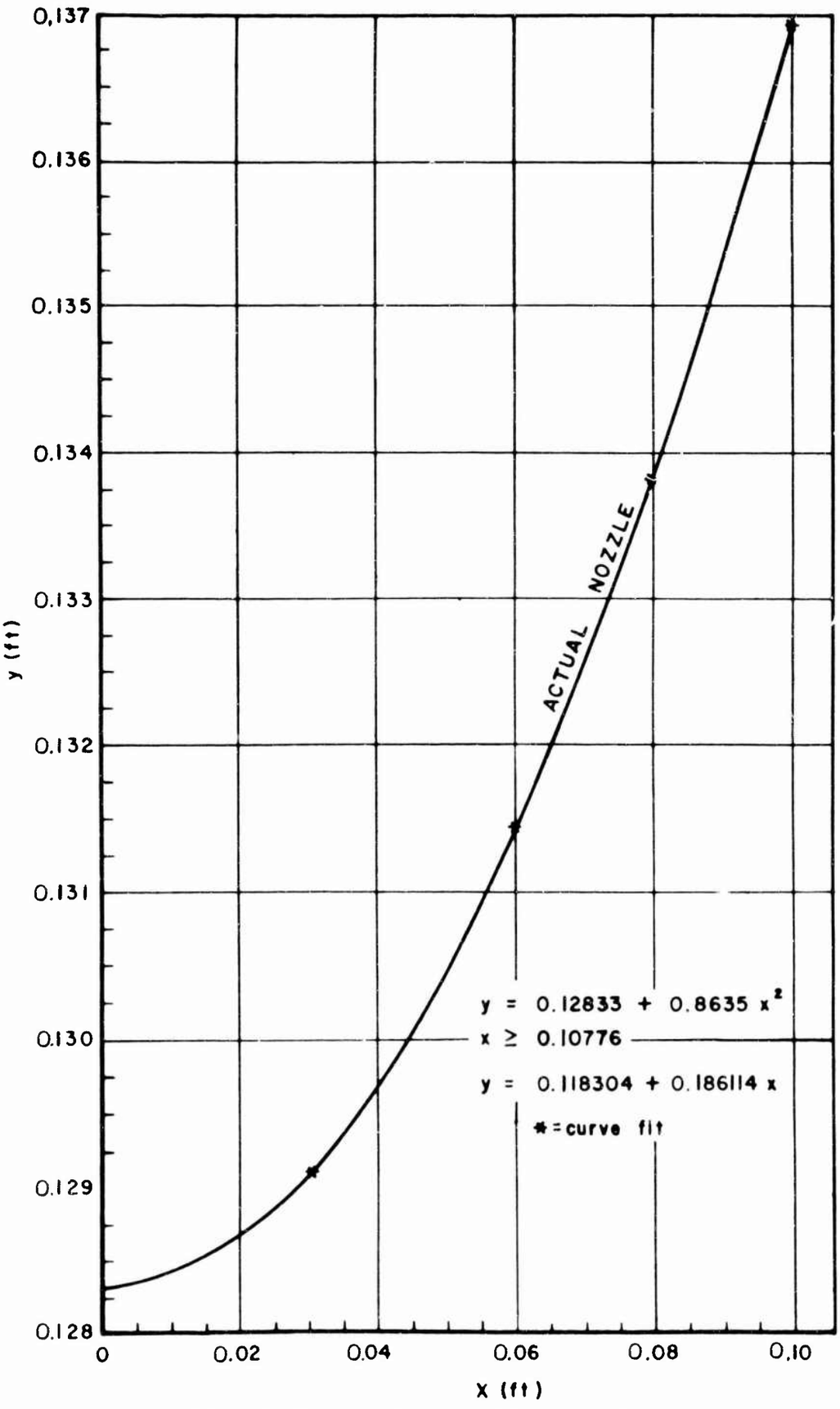

Figure 8. Actual Nozzle Contour Curve and Equation Used in Computer to Duplicate Curve

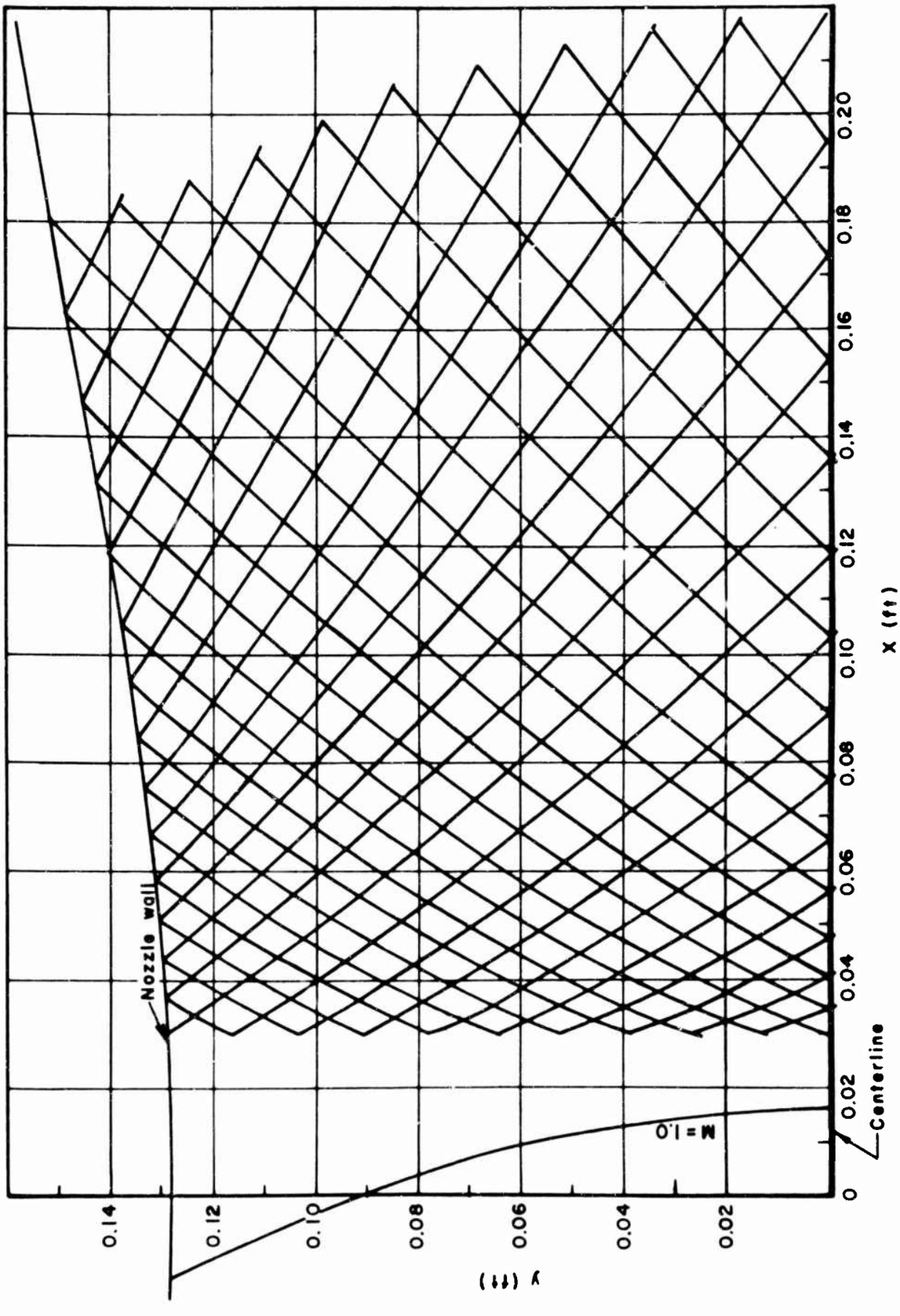

Figure 9. Characteristic Net for Axisymmetric Nozzle

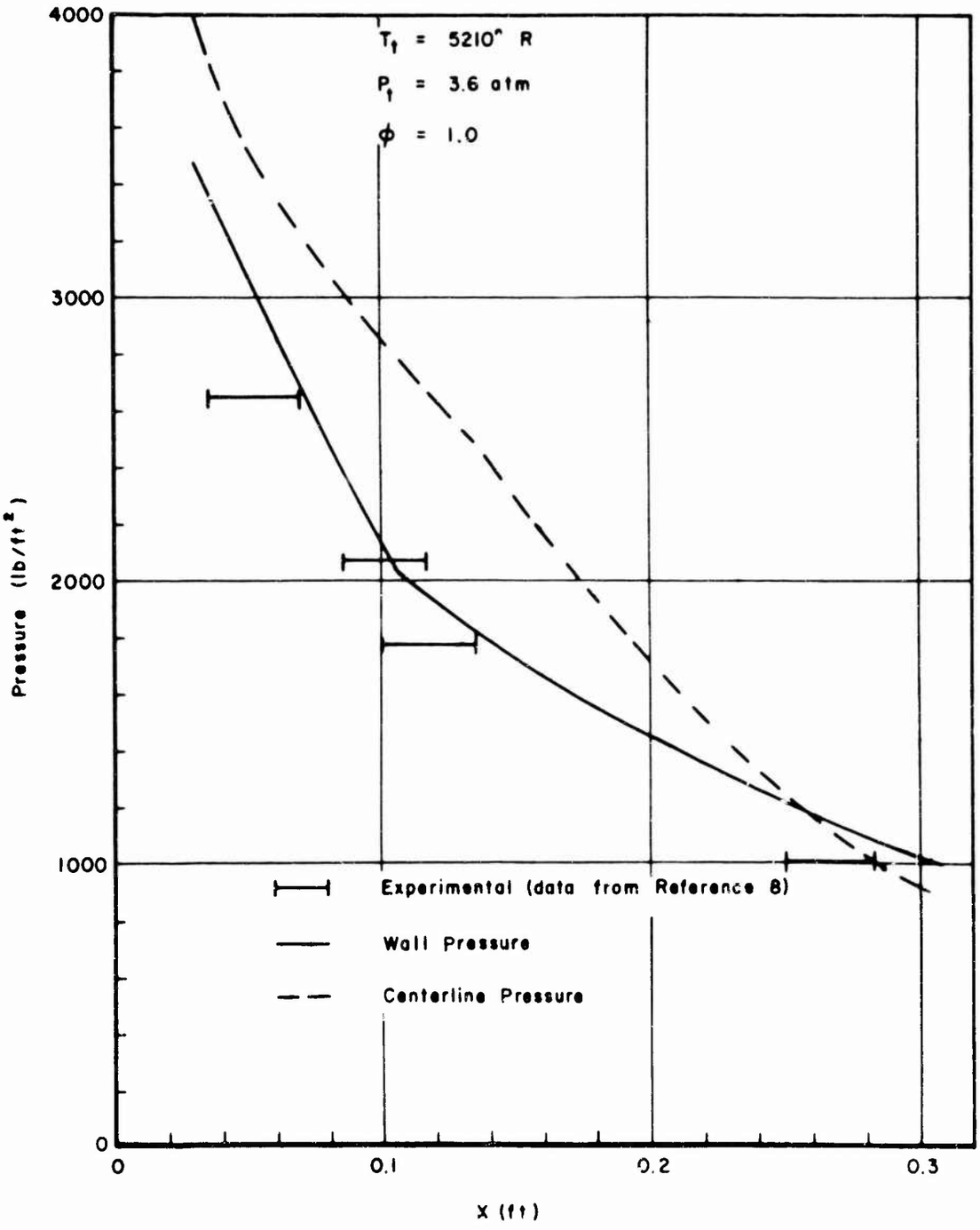

Figure 10. Comparison of Theoretical Pressure Distribution with Experimental Data

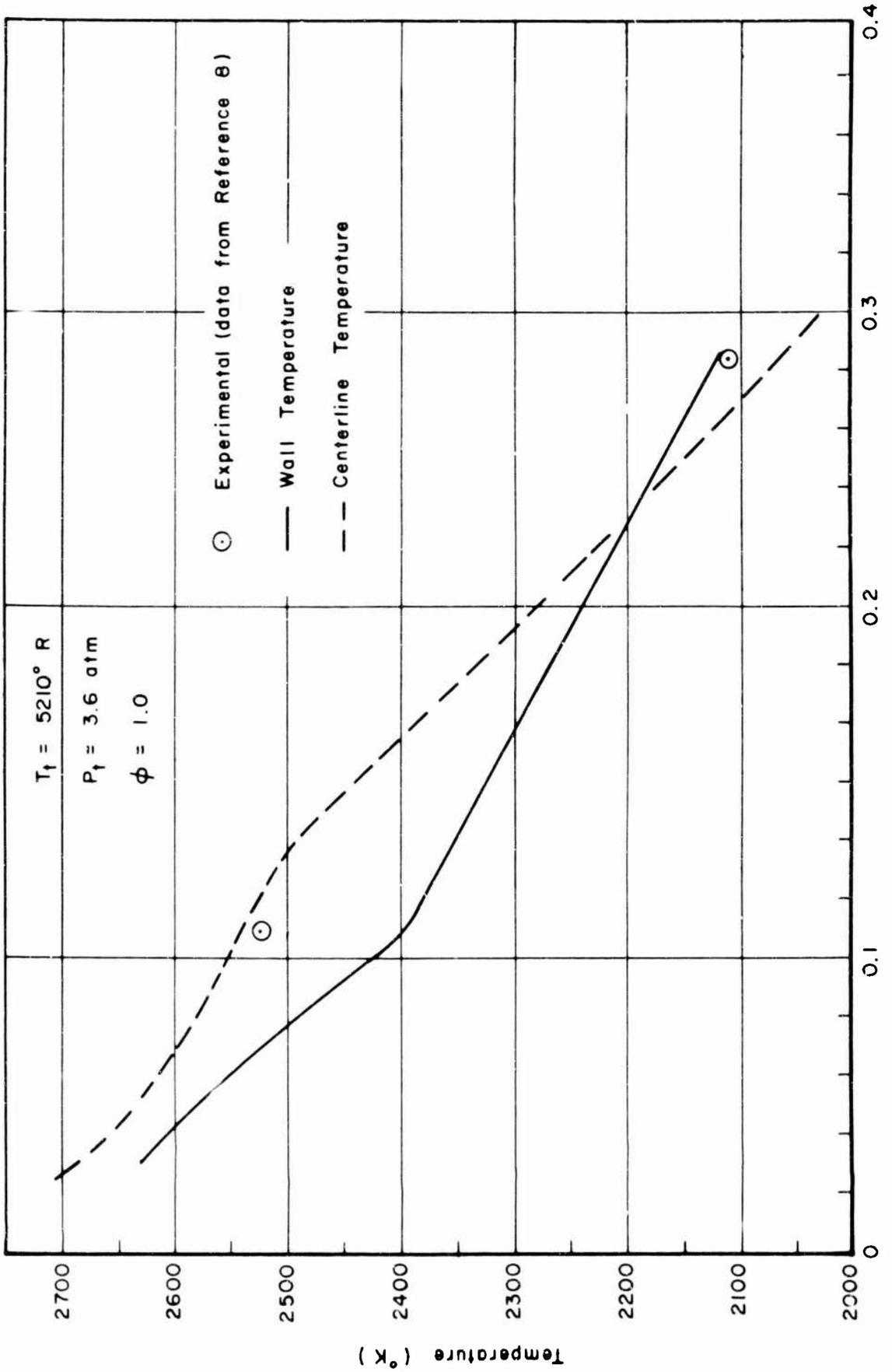

Figure 11. Comparison of Theoretical Temperature Distribution with Experimental Data

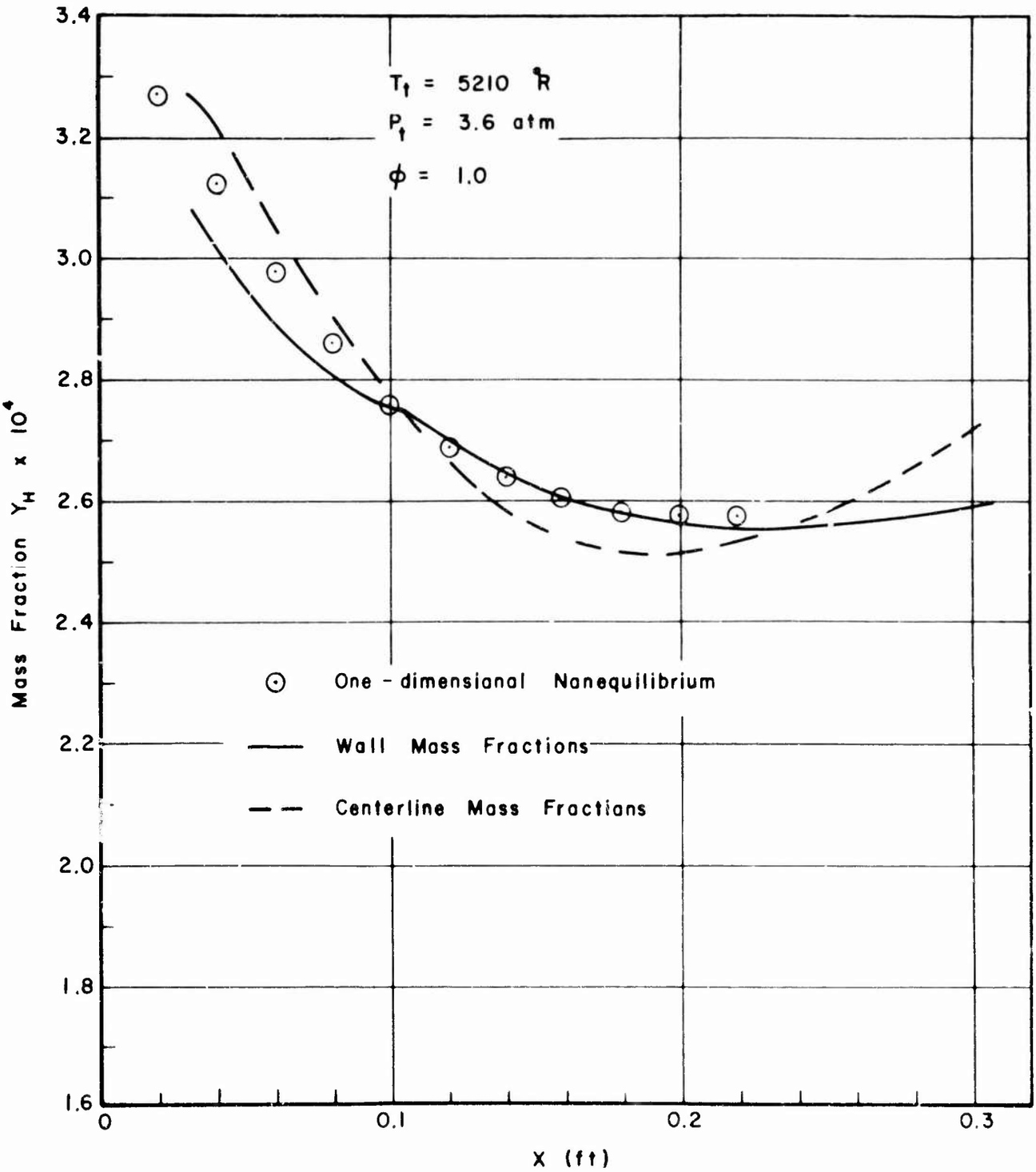

Figure 12. Variation in Mass Fraction of H for Axisymmetric Nozzle

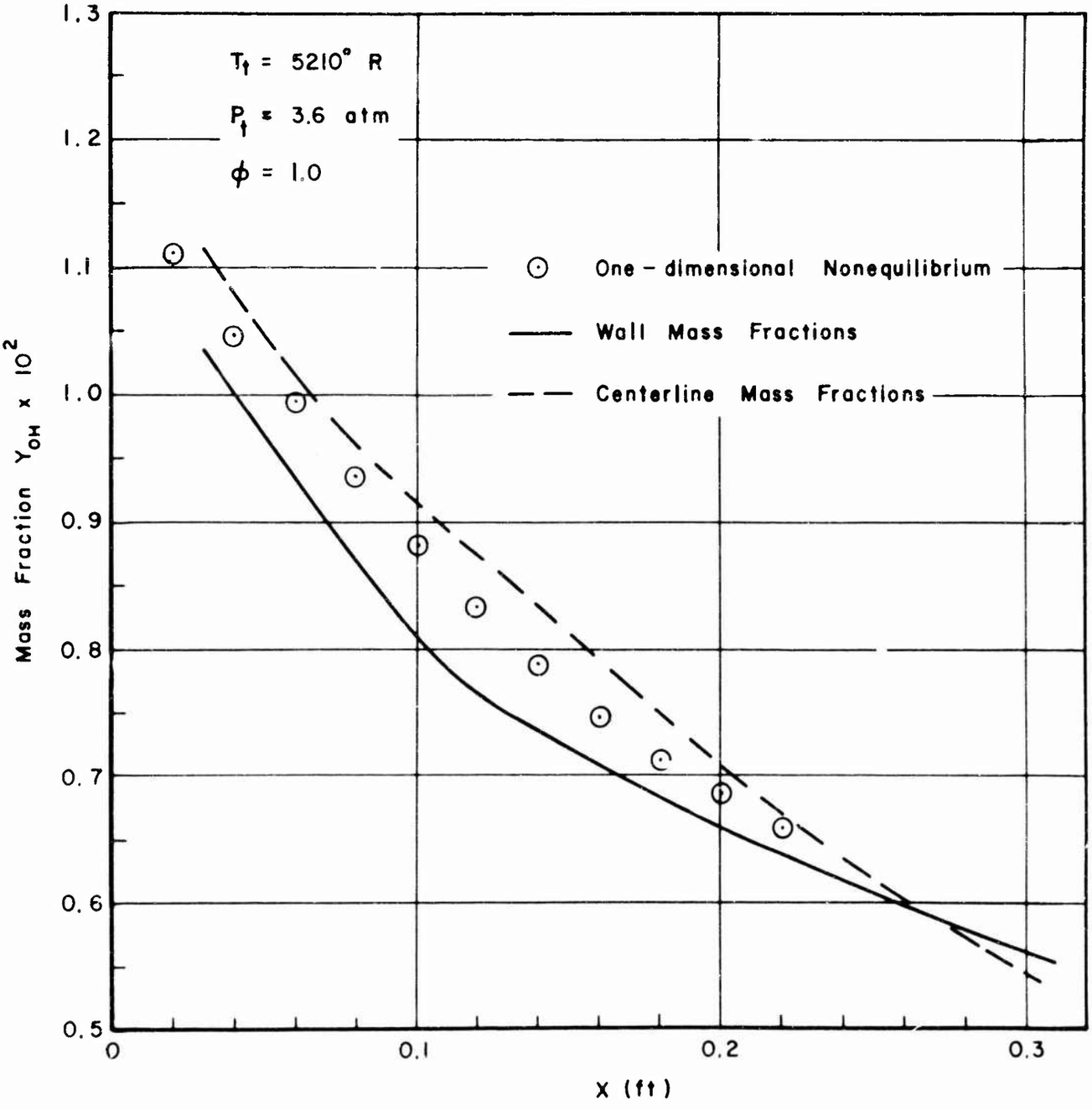

Figure 13. Variation in Mass Fraction of OH for Axisymmetric Nozzle

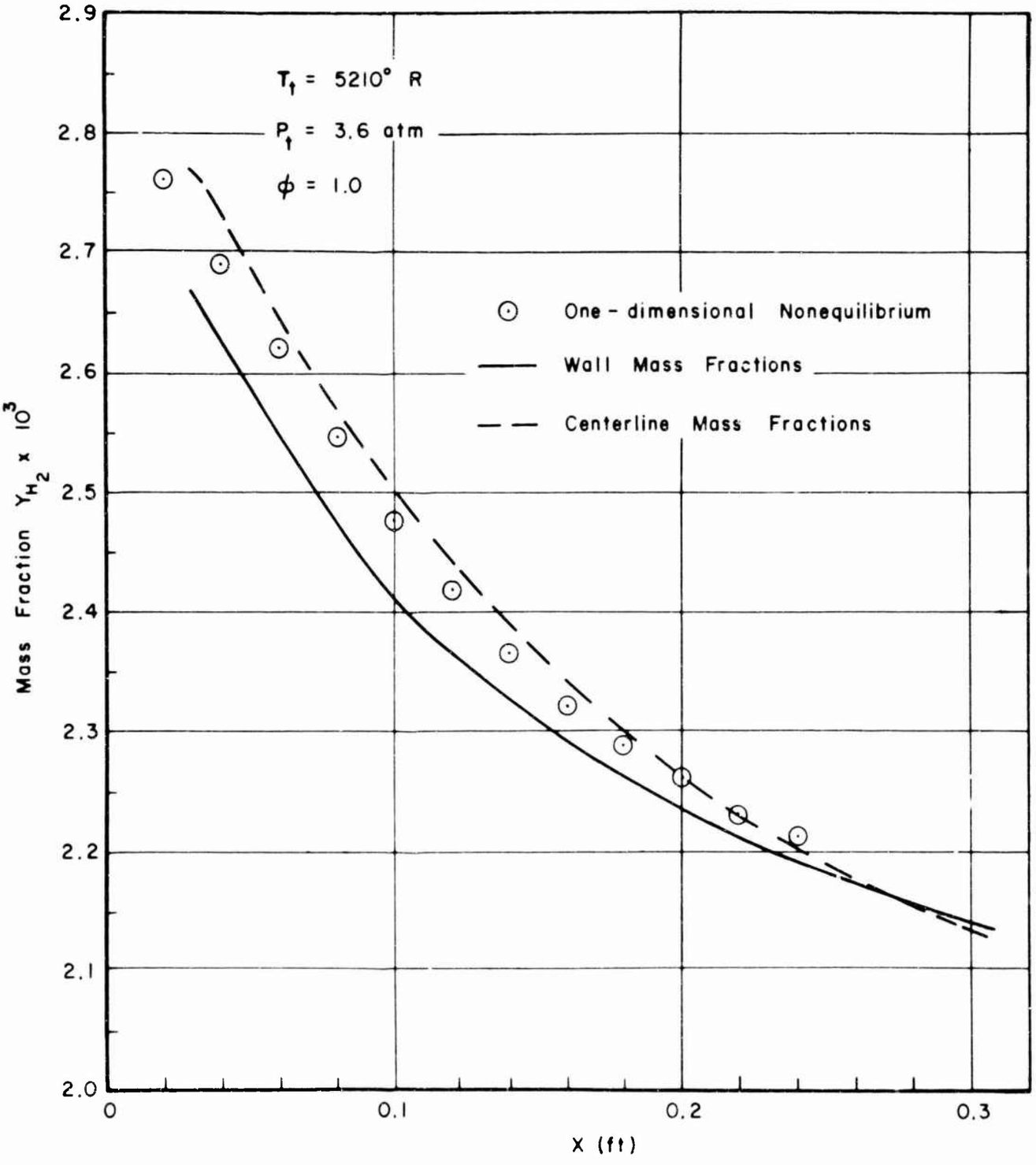

Figure 14. Variation in Mass Fraction of H_2 for Axisymmetric Nozzle

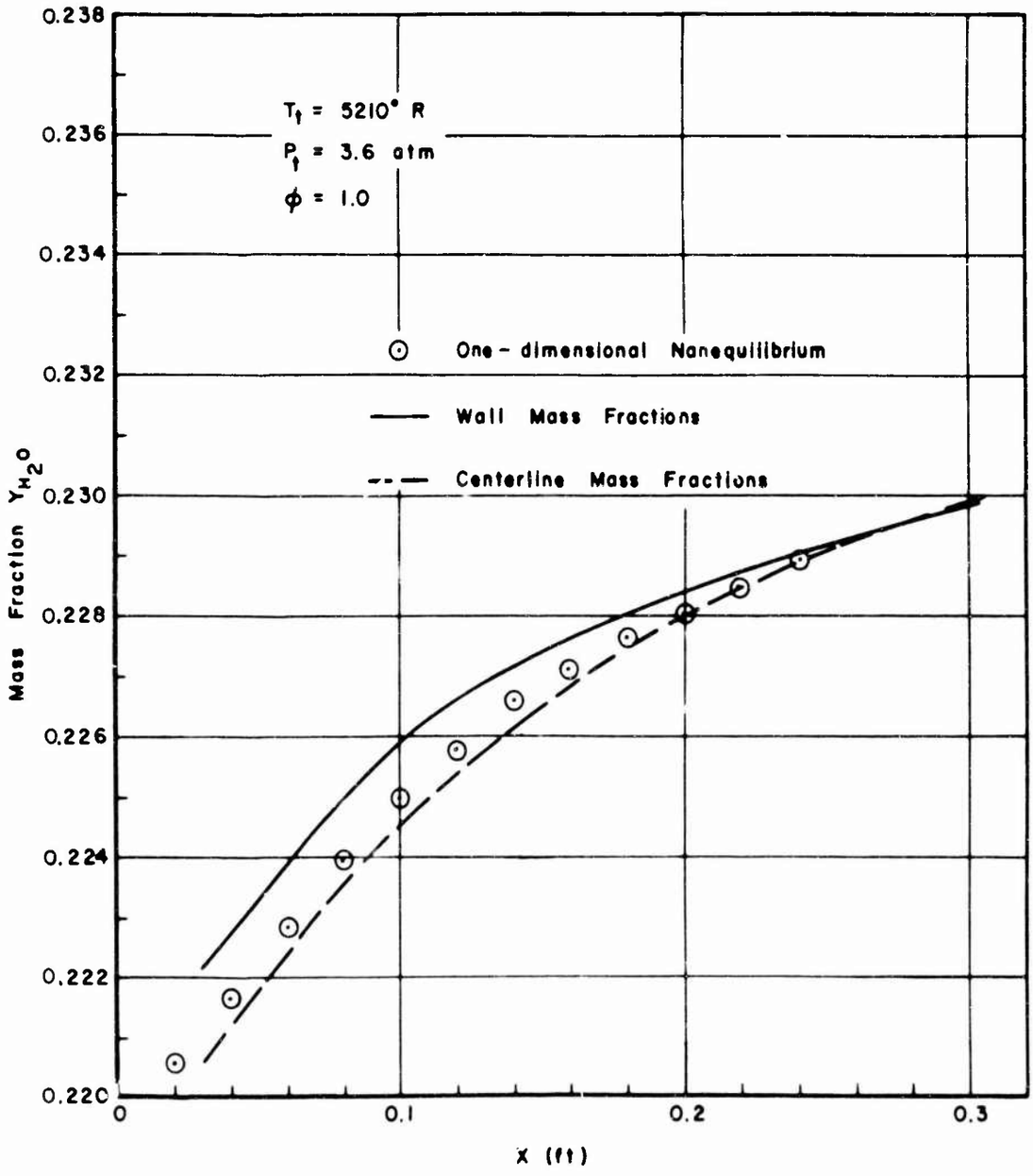

Figure 15. Variation in Mass Fraction of H_2O for Axisymmetric Nozzle

SECTION V

CONCLUSIONS

Through the use of a recently developed computer program, the method of characteristics has successfully been applied to the computation of the flow field of a chemically reacting gas in a DeLaval nozzle. The accomplishment enables one to solve two-dimensional and axisymmetric reactive flow fields.

Excellent agreement was obtained between the computed flow properties and the experimental data for the $N_2O_4 + N_2 \rightleftharpoons 2NO_2 + N_2$ system. Good agreement was obtained with the experimental pressure data for the hydrogen-air system. No direct comparison with the temperature measurements of Reference 8 was possible since the temperatures measured were average temperatures and not specifically the centerline or wall temperature. However, at the second temperature measuring station (Figure 7), the calculated temperature profile was fairly uniform and agreed quite well with the measured temperature.

In addition to analyzing chemically reacting nozzle flows, one can use the program for examining the combustion of a premixed supersonic hydrogen-air mixture. The program also provides a useful standard that can be used to compare approximate methods such as those developed in Reference 11.

REFERENCES

1. B. T. Chu. Wave Propagation and Method of Characteristics in Reacting Gas Mixtures with Applications to Hypersonic Flow. WADC Technical Note 57-213. Prepared by Brown University on Contract AF 33(616)-2798. Aeronautical Research Laboratory, Wright Air Development Center, Wright-Patterson Air Force Base, Ohio. May 1957. (ASTIA Document No. 118,350)

2. W. Lick. Inviscid Flow Around a Blunt Body of a Reacting Mixture of Gases. AFOSR Technical Note 58-522. Office of Scientific Research. May 1958. (ASTIA Document No. 158,335)

3. Peter P. Wegener and Julian D. Cole. Experiments on the Propagation of Weak Disturbances in Stationary Supersonic Flow of Chemically Reacting Gas Mixtures. Progress Report 20-134. Prepared by Jet Propulsion Laboratory, California Institute of Technology, on Contract DA-04-495-ORD-18. Department of the Army. April 1960. (ASTIA Document No. 252,843)

4. Harvey Blend. An Untrasonic Investigation of the Dissociation Kinetics of Nitrogen Tetroxide. Report 19. Department of Physics, University of California. August 1962. (ASTIA Document No. 283,964)

5. Peter P. Wegener. Study of Supersonic Flow with Chemical Reactions. Part II Supersonic Nozzle Flow with a Reacting Gas Mixture at High Reactant Concentration. Progress Report 20-370. Prepared by Jet Propulsion Laboratory, California Institute of Technology, on Contract DA-04-495-ORD-18. Department of the Army. 1958.

6. Gary L. Schott. "Kinetic Studies of Hydroxyl Radicals in Shock Waves. Part III, The OH Concentration Maximum in the Hydrogen Oxygen Reaction." Journal of Chemical Physics. Vol. 32. 1960. P 710.

7. C. B. Ludwig. Chemical Kinetics of Shock Heated Air. Convair Report ZPH-082. Prepared by Convair-San Diego on Contract DA-04-495-ORD-3112. Department of the Army. 1961.

8. E. A. Lezberg and R. B. Lancashire. Recombination of Hydrogen-Air Combustion Products in an Exhaust Nozzle. NASA Technical Note D-1052. Lewis Research Center, National Aeronautics and Space Administration. 1961.

9. R. Sauer. General Characteristics of the Flow Through Nozzles at Near Critical Speeds. NACA TM 1147. National Advisory Committee for Aeronautics. 1947.

10. K. G. Guderley. Aeronautical Research Laboratories (ARM), Wright-Patterson Air Force Base, Ohio.

11. L. Walitt. Marquardt Corporation Memorandum Report 25,067. Prepared by Marquardt Corporation. 1963.